Article

Testing Geometrical Discrimination within an Enzyme Active Site: Constrained Hydrogen Bonding in the Ketosteroid Isomerase Oxyanion Hole

Paul A. Sigala, Daniel A. Kraut, Jose M. M. Caaveiro, Brandon Pybus, Eliza A. Ruben, Dagmar Ringe, Gregory A. Petsko, and Daniel Herschlag

J. Am. Chem. Soc., **2008**, 130 (41), 13696-13708 • DOI: 10.1021/ja803928m • Publication Date (Web): 23 September 2008

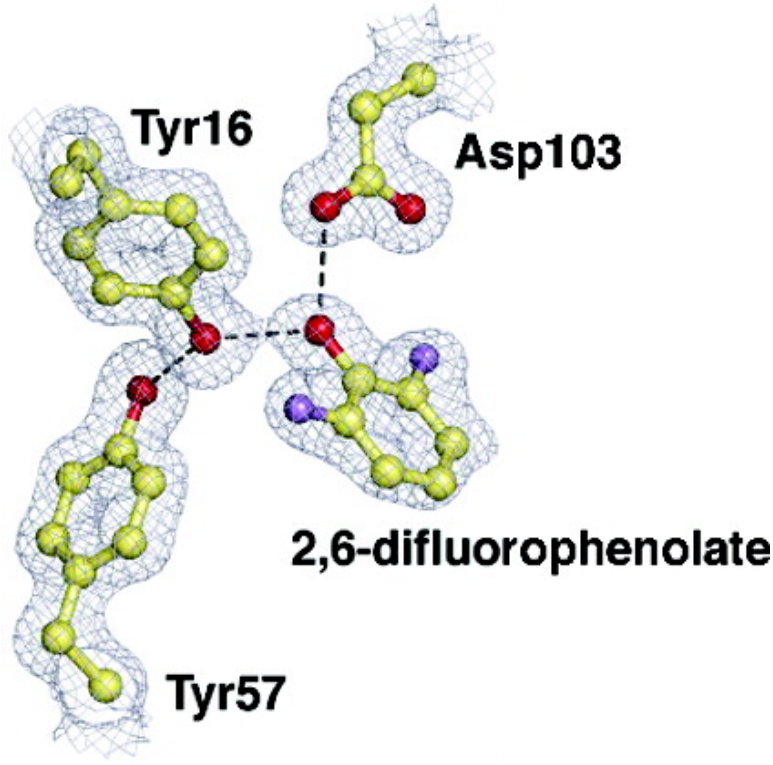

More About This Article

Additional resources and features associated with this article are available within the HTML version:

- Supporting Information
- Links to the 1 articles that cite this article, as of the time of this article download

J|A|C|S
ARTICLES

Published on Web 09/23/2008

Testing Geometrical Discrimination within an Enzyme Active Site: Constrained Hydrogen Bonding in the Ketosteroid Isomerase Oxyanion Hole

Paul A. Sigala,[†] Daniel A. Kraut,[†,§] Jose M. M. Caaveiro,[‡,#] Brandon Pybus,[‡] Eliza A. Ruben,[†] Dagmar Ringe,[‡] Gregory A. Petsko,[‡] and Daniel Herschlag*[,†]

Department of Biochemistry, Stanford University, Stanford, California 94305, and Departments of Biochemistry and Chemistry and Rosenstiel Basic Medical Sciences Research Center, Brandeis University, Waltham, Massachusetts 02454

Received May 26, 2008; E-mail: herschla@stanford.edu

Abstract: Enzymes are classically proposed to accelerate reactions by binding substrates within active-site environments that are structurally preorganized to optimize binding interactions with reaction transition states rather than ground states. This is a remarkably formidable task considering the limited 0.1−1 Å scale of most substrate rearrangements. The flexibility of active-site functional groups along the coordinate of substrate rearrangement, the distance scale on which enzymes can distinguish structural rearrangement, and the energetic significance of discrimination on that scale remain open questions that are fundamental to a basic physical understanding of enzyme active sites and catalysis. We bring together 1.2−1.5 Å resolution X-ray crystallography, ^{1}H and ^{19}F NMR spectroscopy, quantum mechanical calculations, and transition-state analogue binding measurements to test the distance scale on which noncovalent forces can constrain the structural relaxation or translation of side chains and ligands along a specific coordinate and the energetic consequences of such geometric constraints within the active site of bacterial ketosteroid isomerase (KSI). Our results strongly suggest that packing and binding interactions within the KSI active site can constrain local side-chain reorientation and prevent hydrogen bond shortening by 0.1 Å or less. Further, this constraint has substantial energetic effects on ligand binding and stabilization of negative charge within the oxyanion hole. These results provide evidence that subtle geometric effects, indistinguishable in most X-ray crystallographic structures, can have significant energetic consequences and highlight the importance of using synergistic experimental approaches to dissect enzyme function.

Introduction

Enzymes and the chemical transformations they catalyze are central to all biological processes, and enzymes have evolved within the aqueous intracellular environment to accelerate reactions by greater than 20 orders of magnitude relative to the rates of the uncatalyzed reactions in water.[1] Enormous progress has been made over the past 50 years in elucidating the three-dimensional structures, key catalytic groups, and chemical mechanisms of enzymes. Nonetheless, a comprehensive understanding of the physical basis for enzymatic rate enhancement remains a critical challenge of biochemistry and a key hurdle to successful rational design of novel enzymes with desired catalytic properties.[2−5] Attaining a deeper understanding of the catalytic power of enzymes will require experimental tests of the physical properties of active sites that go well beyond structural snapshots and the rate effects from removal of reactive groups.

One of the most basic and widely discussed properties of an enzyme active site is the orientation of its constituent backbone and side-chain groups during folding to create a highly structured and idiosyncratic environment. Noncovalent contacts with neighboring active-site residues position bound substrates relative to each other and relative to reactive functional groups. Indeed, Polanyi, Pauling, Haldane, and others proposed early on that enzyme active sites are structurally preorganized so as to complement and preferentially bind reaction transition states rather than ground states.[6−11] Experimental evidence for the transition-state complementarity of active sites comes from the tight binding of inhibitors that structurally and/or electrostatically resemble expected transition states rather than ground states.[10,11] Numerous structural studies have also revealed active-site pockets that appear spatially organized to optimize transition-

[†] Stanford University.
[‡] Brandeis University.
[§] Present address: Department of Biochemistry, Molecular Biology & Cell Biology, Northwestern University.
[#] Present address: Laboratory of Physical Biochemistry, Graduate School of Frontier Sciences, University of Tokyo, Japan.

(1) Lad, C.; Williams, N. H.; Wolfenden, R. *Proc. Natl. Acad. Sci. U.S.A.* **2003**, *100*, 5607–5610.
(2) Bolon, D. N.; Voigt, C. A.; Mayo, S. L. *Curr. Opin. Chem. Biol.* **2002**, *6*, 125–129.
(3) Jiang, L.; Althoff, E. A.; Clemente, F. R.; Doyle, L.; Rothlisberger, D.; Zanghellini, A.; Gallaher, J. L.; Betker, J. L.; Tanaka, F.; Barbas, C. F., III; Hilvert, D.; Houk, K. N.; Stoddard, B. L.; Baker, D. *Science* **2008**, *319*, 1387–1391.
(4) Kaplan, J.; DeGrado, W. F. *Proc. Natl. Acad. Sci. U.S.A.* **2004**, *101*, 11566–11570.
(5) Lippow, S. M.; Tidor, B. *Curr. Opin. Biotechnol.* **2007**, *18*, 305–311.

10.1021/ja803928m CCC: $40.75

Scheme 1. Geometric and Electrostatic Changes in (A) the Carbonyl C−O during Peptide Bond Hydrolysis and (B) Nonbridging Oxygen Atoms during Phosphoryl Transfer Reactions (Nucleophile Not Shown) Going from the Ground State (Black) to the Transition State (Red)

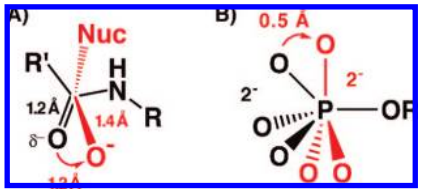

state interactions, including the placement of charged residues and hydrogen bond donors that appear to anticipate the approach of complementary charges and hydrogen bond acceptors in the transition state.[9,12−15] This widely proposed ability of active-site groups to preferentially interact with specific substrate moieties in the transition state versus the ground state rests on the changes in charge distribution and atomic positions that occur within reacting substrates along the reaction coordinate, as illustrated in the following examples.

During peptide bond hydrolysis, the carbonyl C−O bond lengthens from 1.2 Å in the ground state to 1.4 Å in the transition state as negative charge localizes on the oxygen and C−O bond order decreases. This lengthening is accompanied by a ∼1.2 Å spatial translation of the carbonyl oxygen (relative to the carbonyl carbon) due to rehybridization of the carbonyl carbon from sp^2 in the planar ground state to sp^3 in the tetrahedral transition state (Scheme 1A).[16−18] Similarly, during phosphoryl-transfer reactions, the nonbridging oxygen atoms translate ∼0.5 Å through space as the phosphoryl group progresses from a tetrahedral ground state to a trigonal bipyramidal transition state (Scheme 1B).[19,20]

It was therefore reasoned that, if enzymatic groups were positioned with sufficient rigidity to limit their spatial fluctuations relative to the scale of substrate rearrangement, then binding interactions between these groups and substrate atoms undergoing changes in charge localization and position during catalysis could not be optimal with both the ground-state and transition-state configurations of the reacting substrate.[11,13] Based on these considerations, a substantial portion of enzymatic

Scheme 2. Schematic Depiction of Proposed Optimization of Transition-State Rather than Ground-State Binding within (A) Serine Protease and (B) Protein Tyrosine Phosphatase Active Sites

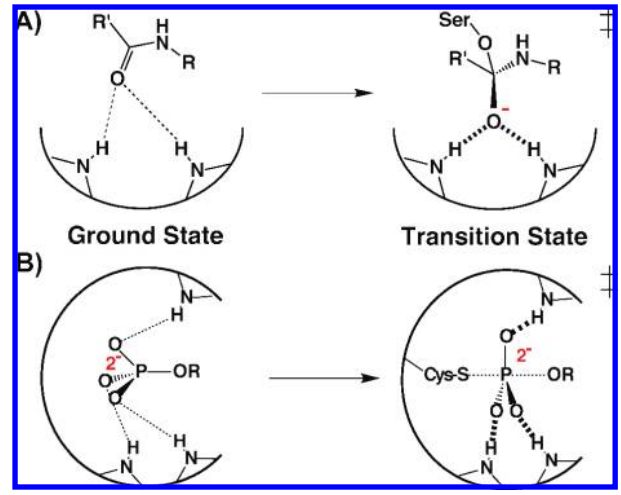

rate enhancement is classically proposed to result from binding substrates within active-site environments that are structurally preorganized to optimize binding interactions with reaction transition states rather than ground states.[6−9,11,21] This optimization is illustrated in Scheme 2 for proposed interactions within serine protease[14,15] and protein tyrosine phosphatase[19,22,23] active sites. Nonetheless, experimental evaluation of whether active-site groups are positioned with sufficient rigidity to differentially interact with substrate atoms undergoing 0.1−1 Å spatial translations during catalysis remains a fundamental challenge, the significance and history of which we further address below.

Initial proposals regarding the catalytic importance of transition-state complementarity envisioned enzymes to have sufficiently rigid active sites such that large forces could be brought to bear on bound substrate molecules in the ground state, straining and deforming them along specific coordinates toward the transition state.[7,8,24] Early computational modeling of the lysozyme active site, however, suggested that the forces required to significantly distort the rigid covalent bonds within substrates vastly exceeded the much softer van der Waals forces involved in positioning active-site groups. Hence, it appeared physically improbable that sufficient force could be generated by noncovalent binding interactions to significantly distort substrates bound at an enzyme active site.[25]

Nonetheless, several lines of experimental evidence have suggested that covalent bond distortions on the scale of ∼0.5 Å or smaller are possible within an enzyme active site. These studies provide evidence that groups can be positioned with sufficient rigidity to prevent plastic rearrangement of local active-site architecture that would otherwise dissipate the local forces required for distortion. High- and ultrahigh-resolution X-ray structures have revealed examples of functional groups

(6) Polanyi, M. *Z. Elektrochem.* **1921**, *27*, 142–150.
(7) Pauling, L. *Chem. Eng. News* **1946**, *24*, 1375–1377.
(8) Haldane, J. B. S. *Enzymes*; Longmans, Green: London, 1930.
(9) Jencks, W. P. *Catalysis in Chemistry and Enzymology*, 2nd ed.; Dover: New York, 1987.
(10) Wolfenden, R. *Acc. Chem. Res.* **1972**, *5*, 10–18.
(11) Lienhard, G. E. *Science* **1973**, *180*, 149–154.
(12) Blake, C. C.; Johnson, L. N.; Mair, G. A.; North, A. C.; Phillips, D. C.; Sarma, V. R. *Proc. R. Soc. London B: Biol. Sci* **1967**, *167*, 378–388.
(13) Fersht, A. R. *Structure and Mechanism in Protein Science*, 2nd ed.; W. H. Freeman and Co.: New York, 1999.
(14) Robertus, J. D.; Kraut, J.; Alden, R. A.; Birktoft, J. J. *Biochemistry* **1972**, *11*, 4293–4303.
(15) Fersht, A. R.; Blow, D. M.; Fastrez, J. *Biochemistry* **1973**, *12*, 2035–2041.
(16) Fersht, A. R. *Proc. R. Soc. London B: Biol. Sci* **1974**, *187*, 397–407.
(17) Wilmouth, R. C.; Edman, K.; Neutze, R.; Wright, P. A.; Clifton, I. J.; Schneider, T. R.; Schofield, C. J.; Hajdu, J. *Nat. Struct. Biol.* **2001**, *8*, 689–694.
(18) Katona, G.; Wilmouth, R. C.; Wright, P. A.; Berglund, G. I.; Hajdu, J.; Neutze, R.; Schofield, C. J. *J. Biol. Chem.* **2002**, *277*, 21962–21970.
(19) Alhambra, C.; Wu, L.; Zhang, Z. Y.; Gao, J. *J. Am. Chem. Soc.* **1998**, *120*, 3858–3866.
(20) Schramm, V. L.; Shi, W. X. *Curr. Opin. Struct. Biol.* **2001**, *11*, 657–665.
(21) Wolfenden, R. *Annu. Rev. Biophys. Bioeng.* **1976**, *5*, 271–306.
(22) Zhang, Z. Y.; Wang, Y.; Wu, L.; Fauman, E. B.; Stuckey, J. A.; Schubert, H. L.; Saper, M. A.; Dixon, J. E. *Biochemistry* **1994**, *33*, 15266–15270.
(23) Zhang, M.; Zhou, M.; Van Etten, R. L.; Stauffacher, C. V. *Biochemistry* **1997**, *36*, 15–23.
(24) Lumry, R. *Ann. N.Y. Acad. Sci.* **1974**, *227*, 46–73.
(25) Levitt, M. In *Peptides, polypeptides, and proteins*; Blout, E. R., Bovey, F. A., Goodman, M., Lotan, N., Eds.; Wiley: New York, 1974; pp 99−113.

within enzyme interiors that appear significantly distorted from canonical geometry, presumably due to noncovalent interactions with nearby residues. In several cases, these structures have been solved to sub-angstrom resolution with estimated coordinate uncertainties as low as 0.01 Å (unfettered by the tight geometric restraints usually needed in refinements at lower resolutions), permitting detection of subtle geometric distortions less than 0.5 Å that would be difficult to reliably detect in typical X-ray structures.[26,27] These examples include distortions of sugar conformations from the chair toward the half-chair forms in 1.9, 1.8, and 0.94 Å resolution structures of glycosidases;[28−30] bending of a Phe side chain by 0.3 Å from planarity in a 0.83 Å resolution structure of α-lytic protease;[31] arching of the phenolic chromophore by 0.25 Å from planarity in a 0.82 Å resolution structure of photoactive yellow protein;[32] bending of the flavin ring by 17° in a 0.98 Å resolution cholesterol oxidase structure;[33] and deviations from planarity in peptide bonds by up to 17° in 1.0, 1.1, and 0.66 Å resolution structures of cutinase, elastase, and aldose reductase, respectively.[34−36] In addition, resonance Raman studies of the scissile C═O bond in bound substrates of serine proteases have detected vibrational changes indicative of 0.02−0.03 Å increases in the C═O bond length and suggesting that oxyanion hole groups and bound substrates are positioned with sufficient rigidity to apply force along specific trajectories and effect subtle geometric distortions.[37,38]

The ability of active sites to discriminate geometric differences on the 0.1−1 Å scale, however, is difficult to reconcile with molecular dynamics (MD) simulations and low-temperature X-ray diffraction studies that have revealed that atomic positions within active sites are not static but vary on the order of 0.1−0.5 Å due to individual and collective atomic vibrations and librations.[39−43] Such intrinsic motions may severely limit the ability of active-site groups to distinguish geometric changes in reacting substrates that are of a similar magnitude. It remains possible, however, that limiting motions of active-site groups along a specific trajectory may enhance rigidity along the particular coordinate needed for recognition of substrate rearrangement. Indeed, atomic displacements within covalently bonded groups are highly anisotropic due to stretching, rocking, and bending motions and limits on rotational flexibility inherent to covalent bonds.[41]

As these examples from the literature indicate, the scale of geometric discrimination possible within an enzyme active site and the energetic importance of such discrimination remain unresolved questions that are fundamental to our most basic understanding of how enzymes work. In this work, we bring together high-resolution X-ray crystallography, ^{1}H and ^{19}F NMR spectroscopy, quantum mechanical calculations, and transition-state analogue binding measurements to address two critical questions regarding the nature of geometric discrimination possible within a particular enzyme active site: (1) On what distance scale can forces within an active site constrain the structural relaxation or translation of side chains and ligands along a specified coordinate? (2) What are the energetic consequences of geometric constraints on this scale?

We have exploited the ability to spectroscopically observe short hydrogen bonds in the oxyanion hole of bacterial ketosteroid isomerase (KSI) to ask whether forces arising from noncovalent binding contacts within the active site can constrain hydrogen bonds from shortening to their preferred bond lengths. Our results strongly suggest that packing interactions within the KSI active site can constrain local side-chain reorientation and prevent hydrogen bond shortening by 0.1 Å or less. Furthermore, these constraints appear to have substantial energetic consequences for ligand binding and negative charge stabilization within the oxyanion hole. This work provides evidence that subtle geometric effects, indistinguishable by most X-ray structures, can have substantial energetic consequences, underscoring the importance of combining structural, spectroscopic, and energetic approaches to dissect enzyme function.

Results and Discussion

KSI and the Experimental Approach. Bacterial KSI from *Pseudomonas putida* (pKSI) and *Commamonas testosteroni* (tKSI) catalyzes double-bond isomerization in a wide variety of steroid substrates via formation of a negatively charged dienolate intermediate (Scheme 3A). The intermediate is stabilized by hydrogen bonds within an active-site oxyanion hole composed of Y16 (pKSI numbering) and protonated D103 and is surrounded by a dense constellation of predominantly hydrophobic side chains. Single-ring phenolate anions substituted in the *meta* and *para* positions with electron-withdrawing groups have previously been shown to bind and accept two hydrogen bonds within the KSI oxyanion hole and serve as analogues of the dienolate intermediate and dienolate-like transition states (Scheme 3B).[44,45] The binding of a series of phenolates of constant molecular shape but increasing oxyanion charge localization mimics the analogous charge development in the oxyanion hole during steroid isomerization. A 1.25 Å resolution X-ray structure of unsubstituted phenolate bound to $pKSI^{D40N}$ (this mutation mimics the protonated general base, D40, present in the KSI-intermediate complex) revealed that

(26) Vrielink, A.; Sampson, N. *Curr. Opin. Struct. Biol.* **2003**, *13*, 709–715.
(27) Cachau, R. E.; Podjarny, A. D. *J. Mol. Recognit.* **2005**, *18*, 196–202.
(28) Kuroki, R.; Weaver, L. H.; Matthews, B. W. *Science* **1993**, *262*, 2030–2033.
(29) Sidhu, G.; Withers, S. G.; Nguyen, N. T.; McIntosh, L. P.; Ziser, L.; Brayer, G. D. *Biochemistry* **1999**, *38*, 5346–5354.
(30) Guerin, D. M. A.; Lascombe, M. B.; Costabel, M.; Souchon, H.; Lamzin, V.; Beguin, P.; Alzari, P. M. *J. Mol. Biol.* **2002**, *316*, 1061–1069.
(31) Fuhrmann, C. N.; Kelch, B. A.; Ota, N.; Agard, D. A. *J. Mol. Biol.* **2004**, *338*, 999–1013.
(32) Getzoff, E. D.; Gutwin, K. N.; Genick, U. K. *Nat. Struct. Biol.* **2003**, *10*, 663–668.
(33) Lyubimov, A. Y.; Heard, K.; Tang, H.; Sampson, N. S.; Vrielink, A. *Protein Sci.* **2007**, *16*, 2647–2656.
(34) Longhi, S.; Czjzek, M.; Lamzin, V.; Nicolas, A.; Cambillau, C. *J. Mol. Biol.* **1997**, *268*, 779–799.
(35) Wurtele, M.; Hahn, M.; Hilpert, K.; Hohne, W. *Acta Crystallogr., Sect. D: Biol. Crystallogr.* **2000**, *56*, 520–523.
(36) Howard, E. I.; Sanishvili, R.; Cachau, R. E.; Mitschler, A.; Chevrier, B.; Barth, P.; Lamour, V.; Van Zandt, M.; Sibley, E.; Bon, C.; Moras, D.; Schneider, T. R.; Joachimiak, A.; Podjarny, A. *Proteins: Struct., Funct. Bioinf.* **2004**, *55*, 792–804.
(37) Tonge, P. J.; Carey, P. R. *Biochemistry* **1992**, *31*, 9122–9125.
(38) Whiting, A. K.; Peticolas, W. L. *Biochemistry* **1994**, *33*, 552–561.
(39) Frauenfelder, H.; Petsko, G. A.; Tsernoglou, D. *Nature* **1979**, *280*, 558–563.
(40) Artymiuk, P. J.; Blake, C. C.; Grace, D. E.; Oatley, S. J.; Phillips, D. C.; Sternberg, M. J. *Nature* **1979**, *280*, 563–568.
(41) Ringe, D.; Petsko, G. A. *Methods Enzymol.* **1986**, *131*, 389–433.
(42) Karplus, M.; McCammon, J. A. *Annu. Rev. Biochem.* **1983**, *52*, 263–300.
(43) Ladner, J. E.; Wladkowski, B. D.; Svensson, L. A.; Sjolin, L.; Gilliland, G. L. *Acta Crystallogr., Sect. D: Biol. Crystallogr.* **1997**, *53*, 290–301.
(44) Petrounia, I. P.; Pollack, R. M. *Biochemistry* **1998**, *37*, 700–705.
(45) Kraut, D. A.; Sigala, P. A.; Pybus, B.; Liu, C. W.; Ringe, D.; Petsko, G. A.; Herschlag, D. *PLoS Biol.* **2006**, *4*, e99.

Scheme 3. (A) Mechanism of KSI-Catalyzed Steroid Isomerization, (B) Equilibrium Binding of a Substituted Phenolate from Water into the KSI Active Site, and (C) Schematic Depiction of a Di-*ortho*-F-Substituted Phenolate Bound at the KSI Active Site

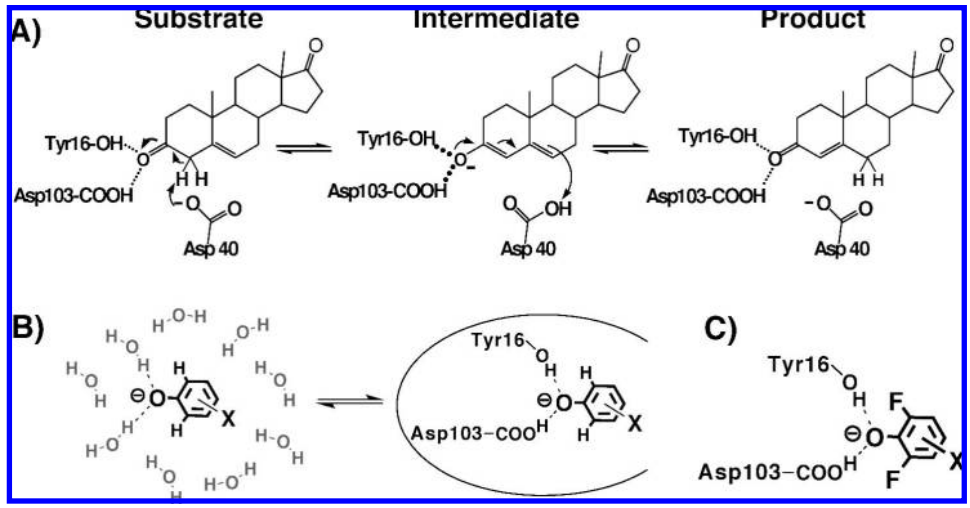

the hydrogen bonds formed to the phenolate oxygen were substantially shorter than the vast majority of 2.8−3.0 Å hydrogen bonds typically observed in protein X-ray structures,[46,47] with average O−O distances of 2.5 and 2.6 Å.[45] Consistent with the short distances observed by X-ray crystallography, the protons bridging these two hydrogen bonds appeared as far downfield peaks (14−18 ppm) in NMR spectra of tKSI^{D40N}·phenolate complexes.[44,45]

The hydrogen-bonded protons in the oxyanion hole become progressively deshielded as the pK_a and negative charge density on the oxygen of the bound phenolate are increased,[48] as expected for proton migration toward the oxyanion acceptor and shortening of the hydrogen bond O···O distance by ∼0.1 Å from pK_a 5.4 to 9.3.[45] Shortened hydrogen bond lengths are commonly regarded as evidence for hydrogen bond strengthening,[49−52] suggesting that shorter hydrogen bonds formed to phenolates of higher pK_a might lead to substantially tighter binding to the KSI active site. In contrast to this expectation, the shortening of oxyanion hole hydrogen bonds upon binding phenolates of increased negative charge localization was accompanied by only a shallow increase in phenolate binding affinity ($\Delta\Delta G = -0.2$ kcal/mol/pK_a unit). This modest change indicated little net energetic benefit from the observed hydrogen bond changes.[45] However, hydrogen bond shortening was correlated with a large favorable increase in binding enthalpy across the same series of phenolates ($\Delta\Delta H = -2.0$ kcal/mol/pK_a unit). This enthalpic increase is consistent with the simplest expectation for the strengthening of hydrogen bonds upon shortening[49] and suggests that physical changes in oxyanion hole hydrogen bonds might nonetheless play an important role in stabilizing negative charge localization within the KSI active site.

To unify these seemingly paradoxical observations, we proposed a physical model for the KSI active site. According to this model, the progressive shortening of oxyanion hole hydrogen bonds provides a favorable enthalpic contribution to binding phenolates of increasing pK_a that offsets an entropic penalty derived from localizing negative charge within an active-site environment that is otherwise insufficiently preorganized and polar to stabilize localized oxyanion charge better than water. If, as our model specifies, the shortening of oxyanion hole hydrogen bonds by 0.02 Å/pK_a unit results in a favorable energetic contribution to phenolate binding, then phenolate analogues that are structurally prevented from forming progressively shortened hydrogen bonds would be predicted to bind more weakly with increasing oxyanion charge (pK_a) rather than slightly more strongly. In other words, $\Delta\Delta G$/pK_a unit for phenolate binding is predicted to be positive rather than slightly negative, as seen for unhindered phenolates that allow hydrogen bond shortening.

Nevertheless, it remained unclear, given the expectation of anisotropic active-site atomic motion on the 0.1−0.5 Å scale (see Introduction), whether groups within the KSI active site would be positioned with sufficient rigidity for noncovalent binding interactions to constrain geometric relaxation along the coordinate required for hydrogen bond shortening of ≤0.1 Å. It was additionally unclear whether geometric constraints on this distance scale would be energetically significant. The close packing of groups within the oxyanion hole observed in the pKSI^{D40N}·phenolate crystal structure suggested that the presence of *ortho* substituents on the phenolate ring might interfere with shortening of oxyanion hole hydrogen bonds. We hypothesized that fluoro substitution in both *ortho* positions of the phenolate ring (Scheme 3C) might be a sufficiently small steric perturbation to permit phenolates to bind and accept hydrogen bonds in the oxyanion hole but prevent further shortening due to close contacts with the electronegative oxygen atoms of Y16 and D103. We utilized a series of substituted phenolates containing −F groups in both *ortho* positions to test (1) whether binding

(46) Anderson, S.; Crossoon, S.; Moffat, K. *Acta Crystallogr., Sect. D: Biol. Crystallogr.* **2004**, *60*, 1008–1016.
(47) Fuhrmann, C. N.; Daugherty, M. D.; Agard, D. A. *J. Am. Chem. Soc.* **2006**, *128*, 9086–9102.
(48) The correlation between phenolate pK_a and the amount of negative charge localized on the phenolate oxygen is supported by quantum calculations (Gross, K. C.; Seybold, P. G. *Int. J. Quantum Chem.* **2001**, *85*, 569–579. Gross, K. C.; Seybold, P. G.; Hadad, C. M. *Int. J. Quantum Chem.* **2002**, *90*, 445–458) and the 0.01 Å decrease in C−O bond length per unit decrease in phenolate pK_a observed in phenolate X-ray structures in the Cambridge Database (unpublished analysis), as expected for increased C−O bond order from withdrawal of electron density from the phenolate oxygen into the ring and substituent groups.
(49) Hibbert, F.; Emsley, J. *Adv. Phys. Org. Chem.* **1990**, *26*, 255–379.
(50) Kumar, G. A.; McAllister, M. A. *J. Org. Chem.* **1998**, *63*, 6968–6972.
(51) Cleland, W. W.; Kreevoy, M. M. *Science* **1994**, *264*, 1887.
(52) Frey, P. A.; Whitt, S. A.; Tobin, J. B. *Science* **1994**, *264*, 1927.

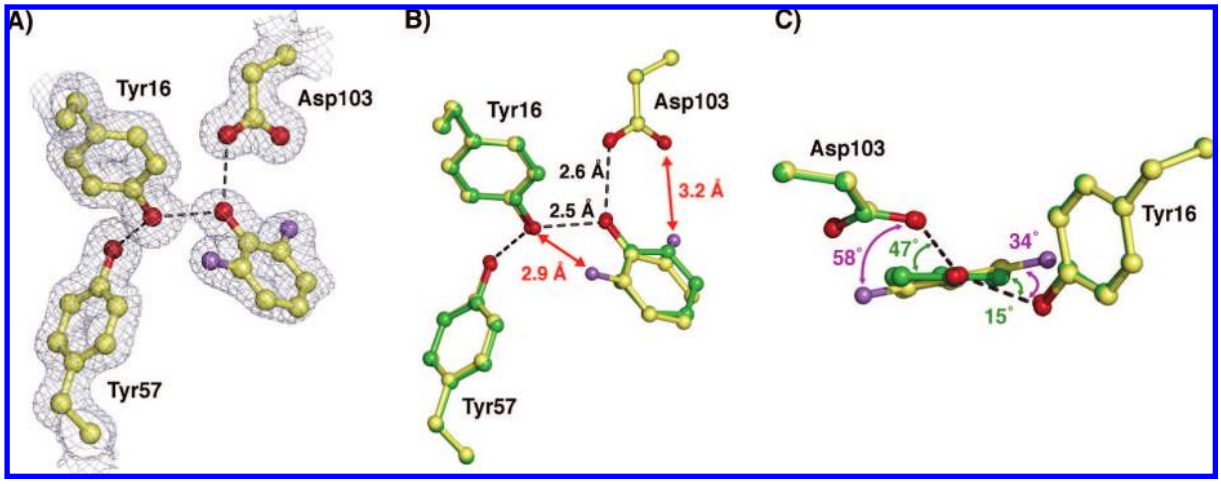

Figure 1. Crystal structure of DFP bound at the active site of pKSI^{D40N}. (A) Sigma-A weighted $2F_o - F_c$ electron density map (contoured at 1.3σ) showing DFP (fluorine atoms in purple) bound in the oxyanion hole, positioned to receive short hydrogen bonds from Tyr16 and Asp103. (B) Superposition of the pKSI^{D40N}·DFP (carbon atoms in yellow) and pKSI^{D40N}·phenolate structures (carbon atoms in green), highlighting the short O···O and O···F distances to DFP. (C) Side-view of the overlay in (B), looking down the phenolate C−O axis, highlighting the different angular displacements for hydrogen bonds formed to the two ligands above and below the plane of the phenolate ring.

interactions between the phenolates and active-site groups can constrain oxyanion hole hydrogen bonds from shortening with increasing pK_a and (2) whether interactions resulting in such a constraint significantly alter the energetics of phenolate binding.

We first determined the crystal structure of 2,6-difluorophenolate (DFP) bound to pKSI^{D40N} to confirm binding and hydrogen bond formation in the oxyanion hole. We then used ^{1}H NMR to assess the change in chemical shift of the observed hydrogen-bonded protons with increasing di-*ortho*-fluorophenolate pK_a. If hydrogen bonds were constrained from shortening in the presence of the *ortho*-F groups, then the chemical shift of the observed proton peaks would vary minimally with increased pK_a. Alternatively, if packing within the KSI active site were insufficiently rigid to prevent plastic rearrangement of local architecture and to occlude hydrogen bond shortening, then hydrogen bond proton chemical shifts would increase with phenolate pK_a, as observed previously. Finally, we assessed the change in binding affinities for a series of di-*ortho*-F-phenolates of increasing pK_a to probe the energetic significance of any detected physical constraint on phenolate binding and hydrogen bond shortening, predicted from our model to result in weaker binding at higher pK_a.

Binding of 2,6-Difluorophenolates in the KSI Oxyanion Hole. UV−vis spectra of di-*ortho*-F-substituted phenols bound to tKSI^{D40N} confirmed binding as anionic phenolates, as observed previously for phenols substituted in only the *meta* or *para* positions (Figure S1, Supporting Information) and as expected for binding in the oxyanion hole.[45] To confirm that DFPs bind in the oxyanion hole within hydrogen-bonding distance to Y16 and D103, the X-ray structure of pKSI^{D40N} cocrystallized with 2,6-difluorophenolate was determined (PDB code 2INX; see Table S1 for complete data collection and refinement statistics). The overall KSI structure obtained at 1.5 Å resolution (R_{work} = 18.5% and R_{free} = 23.4%) is the same as that observed previously for pKSI^{D40N}·phenolate (PDB code 2PZV), with a root-mean-square deviation between the two structures of 0.3 Å for backbone atoms. The electron density map of the pKSI^{D40N}·DFP structure, contoured in Figure 1A at 1.3σ, shows well-defined densities for the modeled atomic positions within the oxyanion hole, with no indication of alternative ligand or side-chain orientations.

The refined positions of the ring and oxygen atoms of the DFP ligand in the X-ray structure are very similar to those observed previously for the bound phenolate ligand, with both oxyanions positioned to receive short hydrogen bonds of ∼2.5 and 2.6 Å from the identically oriented side chains of Tyr16 and Asp103 (Figure 1B). Thus, di-*ortho*-F substitution results in no changes in the observed hydrogen bond O···O distances or side-chain positions within the oxyanion hole detectable at the stated resolutions and 0.06−0.12 Å estimated coordinate error for these two structures. However, reliable detection of geometric changes of 0.1 Å or less would require a coordinate uncertainty of much less than 0.1 Å, as is only achievable in ultrahigh-resolution X-ray structures refined to <1 Å resolution.[53]

Substitution of −F for −H in the *ortho* positions of the phenolate ring increases the bond length from 1.05 Å (C−H) to 1.35 Å (C−F), expands the projection of the van der Waals surface along the C−F bond by 0.6 Å,[54] and replaces the slightly electropositive phenyl−hydrogen with the electronegative phenyl−fluorine.[55] These changes have previously been reported to subtly perturb the structure and energetics of protein interactions.[56−60] The close proximity of the electronegative side-chain oxygens of Y16 and D103 to the expected locations of the *ortho* protons of the phenolate ring observed in the pKSI^{D40N}·phenolate X-ray structure (estimated O···H$_{ortho}$ distances of 2.8 Å for Y16 and 3.1 Å for D103) might be expected to result in significant repulsive interactions upon

(53) Ladd, M. F. C.; Palmer, R. A. *Structure Determination by X-Ray Crystallography*; Kluwer Academic/Plenum Publishers: New York, 2003.
(54) Bondi, A. *J. Phys. Chem.* **1964**, *68*, 441–451.
(55) Auffinger, P.; Hays, F. A.; Westhof, E.; Ho, P. S. *Proc. Natl. Acad. Sci. U.S.A.* **2004**, *101*, 16789–16794.
(56) Xiao, G.; Parsons, J. F.; Tesh, K.; Armstrong, R. N.; Gilliland, G. L. *J. Mol. Biol.* **1998**, *281*, 323–339.
(57) Pal, P. P.; Bae, J. H.; Azim, M. K.; Hess, P.; Friedrich, R.; Huber, R.; Moroder, L.; Budisa, N. *Biochemistry* **2005**, *44*, 3663–3672.
(58) Hammond, S. J.; Birdsall, B.; Feeney, J.; Searle, M. S.; Roberts, G. C.; Cheung, H. T. *Biochemistry* **1987**, *26*, 8585–8590.
(59) Phillips, R. S.; VonTersch, R. L.; Secundo, F. *Eur. J. Biochem.* **1997**, *244*, 658–663.
(60) Park, Y. W.; Luo, J. K.; Schultz, P. G.; Kirsch, J. F. *Biochemistry* **1997**, *36*, 10517–10525.

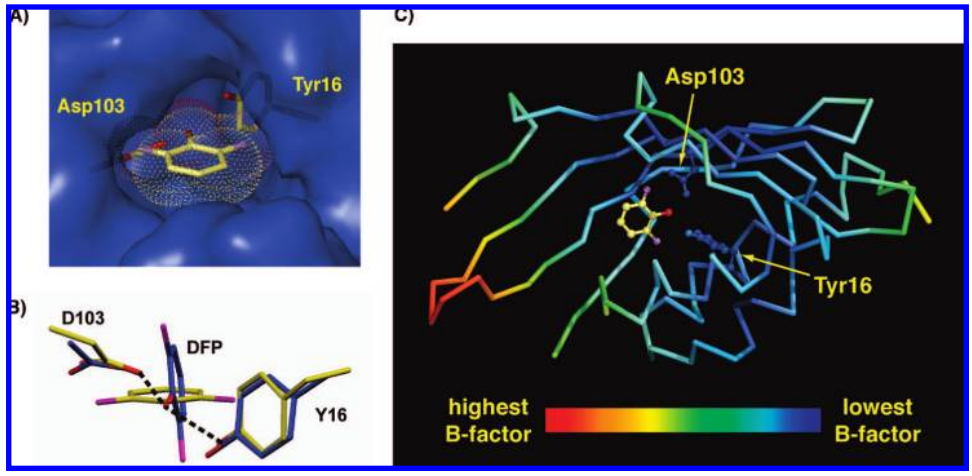

Figure 2. Structural features of KSI-bound DFP and the surrounding binding pocket. (A) Van der Waals protein surface (blue) in the oxyanion hole, showing the close packing of groups around the bound DFP (van der Waals surface shown as dots and colored by atom type: yellow, carbon; red, oxygen; purple, fluorine) and side chains of Asp103 and Tyr16 (yellow). (B) Energy-minimized gas-phase structure (blue) of DFP receiving hydrogen bonds from Y16 (4-Me-phenol) and D103 (acetic acid), calculated at the B3LYP level using the 6-311++G(d,p) basis set, overlaid with the corresponding side-chain and DFP orientations observed in the pKSI^{D40N}·DFP X-ray structure (yellow). (C) pKSI^{D40N} backbone colored according to the highest atomic *B*-factor observed for each residue. The Asp103 and Tyr16 side chains are shown color-coded by their atomic *B*-factors. The DFP ligand is in yellow (not color-coded by *B*-factor).

substitution of the *ortho* protons with larger and strongly electronegative fluorine atoms. Such electrostatic repulsion has previously been reported in theoretical calculations of water−phenolate complexes between the electronegative oxygen of water and coplanar *ortho*-F substituents on the phenolate ring.[61]

While the general orientations of the two ligands within the oxyanion hole are very similar, the DFP ring is rotated ∼15° about its C−O axis such that the angular displacements of the hydrogen bonds formed to Tyr16 and Asp103 out the plane of the phenolate ring are increased from 15° and 47° in the case of phenolate to 34° and 58° in the case of DFP (Figure 1C). This rotation translates the *ortho*-F groups 0.3 Å through space from the positions they would occupy in the absence of rotation (relative to pKSI^{D40N}·phenolate) and increases their distances from the Y16 and D103 oxygens by 0.1−0.3 Å. This rearrangement is consistent with a structural reorientation to relieve O···F repulsive interactions. Further rotation of the phenolate ring appears to be prevented by the close packing of the A118, F86, and D40N side chains and other nearby groups around the bound DFP (Figure 2A). Indeed, quantum calculations of the energy-minimized configuration of DFP receiving hydrogen bonds from Y16 and D103 (modeled as 4-Me-phenol and acetic acid, respectively) suggest that, in the absence of additional surrounding groups, the DFP ligand adopts a configuration nearly perpendicular to that observed in the pKSI^{D40N}·DFP X-ray structure (Figure 2B). This conformation presumably arises in response to electrostatic repulsion between the partial negative charges on the *ortho* fluorines and the nearby side-chain oxygens.

The invariance of the Y16 and D103 side-chain positions in pKSI^{D40N}·DFP relative to pKSI^{D40N}·phenolate (within the 0.1 Å coordinate uncertainty of the structures) appears to reflect local backbone rigidity and the lack of accessible conformations that can increase O···F distances without introducing additional unfavorable contacts with neighboring groups or substantially lengthening the hydrogen bond distance with the phenolate oxyanion. Indeed, residues within the oxyanion hole, especially D103 and the dense milieu of hydrophobic groups immediately surrounding it, have the lowest atomic *B*-factors in the KSI structure (Figure 2C), consistent with lower thermal motions of active-site groups relative to those in other regions of the enzyme.[41] Similarly low *B*-factors for active-site residues are observed in the pKSI^{D40N}·phenolate (Figure S2A) and pKSI^{D40N}·2-F-phenolate (Figure S2B and below) structures, in agreement with previously reported KSI structures.[62] Additional evidence that the mobilities of oxyanion hole groups are restricted relative to other enzyme residues is provided by previous reports that the UV bandwidths corresponding to Y16 are significantly narrower than those of other tyrosine residues in KSI.[63] Hence, the observed orientation of DFP bound to KSI represents the conformational state with the most favorable balance of forces involving oxyanion hole hydrogen bond formation, O···F interactions, and other packing interactions within the KSI active site.

Despite the observed rotation of the DFP ring that appears to increase O···F distances (as discussed above), the 2.9 and 3.2 Å observed distances between the *ortho*-F atoms and oxygens of Y16 and D103 remain similar to the 3.0 Å sum of the van der Waals radii of F (1.5 Å) and O (1.5 Å).[54] This close proximity suggests that repulsive interactions between the partial negative charges on these atoms have not been fully relieved. To test for the presence of significant O···F interactions in the KSI^{D40N}·DFP complex, we acquired ^{19}F NMR spectra of fluorophenolates bound to tKSI^{D40N} and free in solution. The ^{19}F NMR chemical shift of a fluorine atom is dominated by the magnetic shielding conferred by its lone-pair electrons and provides a sensitive probe of local interactions that perturb the distribution of these electrons and hence alter the chemical shift of the fluorine nucleus.[64−66] If repulsive

(61) Andrea, T. A.; Dietrich, S. W.; Murray, W. J.; Kollman, P. A.; Jorgensen, E. C.; Rothenberg, S. *J. Med. Chem.* **1979**, *22*, 221–232.
(62) Oh, K. S.; Cha, S. S.; Kim, D. H.; Cho, H. S.; Ha, N. C.; Choi, G.; Lee, J. Y.; Tarakeshwar, P.; Son, H. S.; Choi, K. Y.; Oh, B. H.; Kim, K. S. *Biochemistry* **2000**, *39*, 13891–13896.
(63) Zhao, Q.; Li, Y. K.; Mildvan, A. S.; Talalay, P. *Biochemistry* **1995**, *34*, 6562.
(64) Gerig, J. T. *Methods Enzymol.* **1989**, *177*, 3–23.
(65) Danielson, M. A.; Falke, J. J. *Annu. Rev. Biophys. Biomol. Struct.* **1996**, *25*, 163–195.

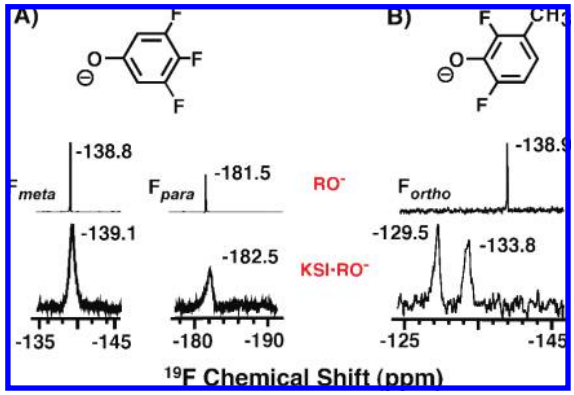

Figure 3. ^{19}F NMR spectra of tKSI^{D40N}·DFP complexes. (A) ^{19}F NMR chemical shifts of the *meta*- and *para*- F atoms in KSI-bound 3,4,5-trifluorophenolate (KSI·RO$^-$) are nearly identical to those of the free phenolate (RO$^-$) in solution at pH 12 (from ref 45). (B) ^{19}F NMR chemical shifts of the *ortho*-F atoms in KSI-bound 3-methyl-2,6-difluorophenolate are perturbed downfield from their values when free in solution.

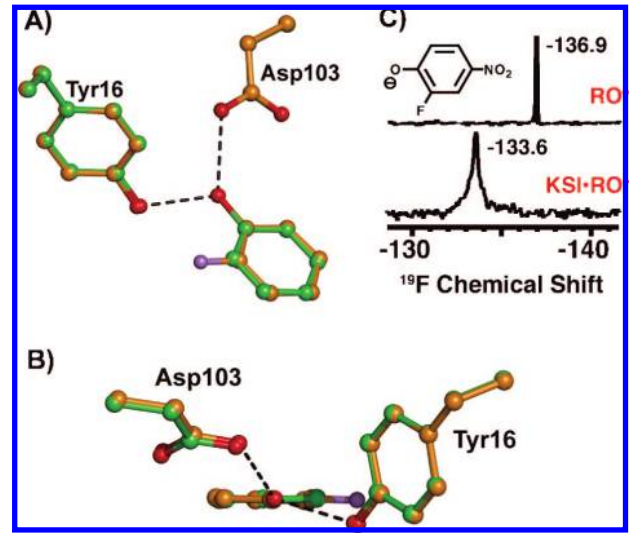

Figure 4. (A) Superposition of the pKSI^{D40N}·2-F-phenolate (orange) and pKSI^{D40N}·phenolate (green) structures. (B) Side view of the overlay in (A), looking down the phenolate C−O axis. (C) ^{19}F NMR spectra of 2-F-4-NO_2-phenolate free in solution at pH 12 (RO$^-$) and bound to tKSI^{D40N} (KSI·RO$^-$).

O···F interactions are present in the KSI^{D40N}·DFP complex, then the ^{19}F chemical shifts of the *ortho*-F atoms are expected to be substantially altered from their values in solution.

Meta- and *para*-substituted fluorophenolates bound to KSI display ^{19}F chemical shifts within ∼1 ppm of their solution values, consistent with their orientation pointing out of the active site, exposure to solvent waters, and the absence of close-packing interactions with nearby residues (Figure 3A and additional fluorophenolate spectra not shown). KSI-bound DFPs, however, display ^{19}F chemical shifts perturbed 5−9 ppm from their solution values, as expected for repulsive interactions between the *ortho*-F atoms and the nearby oxygen atoms of D103 and Y16. The presence of two peaks separated by 4.3 ppm in the ^{19}F NMR spectrum of tKSI^{D40N}·3-Me-DFP (Figure 3B) indicates that the two *ortho*-F atoms experience different local environments when bound within the anisotropic KSI active site proximal to either D103 or Y16.

If there are differential interactions between the two *ortho*-F atoms and the distinct protein groups surrounding them and a corresponding energetic preference for accommodating the *ortho*-F atom of a bound phenolate nearer to Y16 or D103, then a phenolate bearing a single *ortho*-F atom would be expected to bind in the KSI oxyanion hole with the fluorine preferentially oriented toward the side chain, giving rise to the least unfavorable interactions. To test this possibility, the X-ray structure of pKSI^{D40N} cocrystallized with 2-F-phenol was determined (PDB code 3CPO; data collection and refinement statistics listed in Table S2). The final structure, obtained at 1.2 Å resolution (R_{work} = 16.6% and R_{free} = 20.0%), indicates a phenolate binding mode nearly identical to and coplanar with pKSI^{D40N}·phenolate, without rotation about the phenolate C−O bond axis and with the single *ortho*-F atom positioned exclusively on the side of Y16 (Figure 4A,B, electron density map shown in Figure S3). This result suggests that the observed rotation in the DFP structure occurs as a consequence of the O···F contact with the D103 carbonyl oxygen and is consistent with the O···F contact with Y16 giving rise to a smaller repulsive interaction. Furthermore, this result predicts a smaller ^{19}F chemical shift perturbation for the *ortho*-F atom of DFP nearest Y16 than for the −F atom contacting D103. Indeed, the ^{19}F spectrum of tKSI^{D40N}·2-F-4-NO_2-phenol (Figure 4C) reveals a single −F peak perturbed 3.3 ppm downfield from its solution chemical shift, similar to the 5 ppm downfield shift of the less perturbed peak in the tKSI^{D40N}·3-Me-DFP spectrum (Figure 3B). This result supports assignment of the ^{19}F peak shifted 9.4 ppm downfield in the DFP spectrum and the larger O···F repulsive interaction to the contact with the D103 carbonyl oxygen. This larger perturbation may derive from the sp^2 lone-pair orbital on the carbonyl oxygen of D103 that is expected to point toward the nearby fluorine atom, whereas the sp^3 lone pairs on the Y16 oxygen are expected to point substantially away from the proximal fluorine (Figure 1C).

As stated above, our experimental goal was to first verify that DFPs bind and accept hydrogen bonds in the KSI active site and then ask whether packing within the active site is sufficiently rigid for repulsive forces between nearby groups and the *ortho*-F atoms to prevent hydrogen-bonded O···O distances from shortening by 0.1 Å or less. The pKSI^{D40N}·DFP X-ray structure confirmed that DFPs bind in the KSI oxyanion hole within hydrogen-bonding distance of Y16 and D103 but with interactions between the electronegative *ortho*-F atoms and electronegative side-chain oxygens strongly suggested by ^{19}F NMR measurements and computational modeling to be repulsive in nature. We next turned to ^{1}H NMR to directly detect the hydrogen-bonded protons and to test whether the O···F contacts observed in the crystal structure constrain hydrogen bonds formed to the bound DFP from shortening with increasing phenolate pK_a.

Hydrogen Bonds Formed to 2,6-Difluorophenolates Are Constrained from Shortening with Increasing Oxyanion Charge Localization. Structural studies of O−H···O hydrogen bonds in small-molecule complexes by low-temperature neutron diffraction have identified that the bridging proton progressively migrates toward the acceptor oxygen as the O···O separation distance decreases and the donor O−H bond lengthens.[49,67,68] Solid-state and solution NMR studies of the same complexes

(66) Lau, E. Y.; Gerig, J. T. *J. Am. Chem. Soc.* **2000**, *122*, 4408–4417.
(67) Steiner, T.; Saenger, W. *Acta Crystallogr., Sect. B: Struct. Sci.* **1994**, *50*, 348–357.
(68) Gilli, P.; Bertolasi, V.; Ferretti, V.; Gilli, G. *J. Am. Chem. Soc.* **1994**, *116*, 909–915.

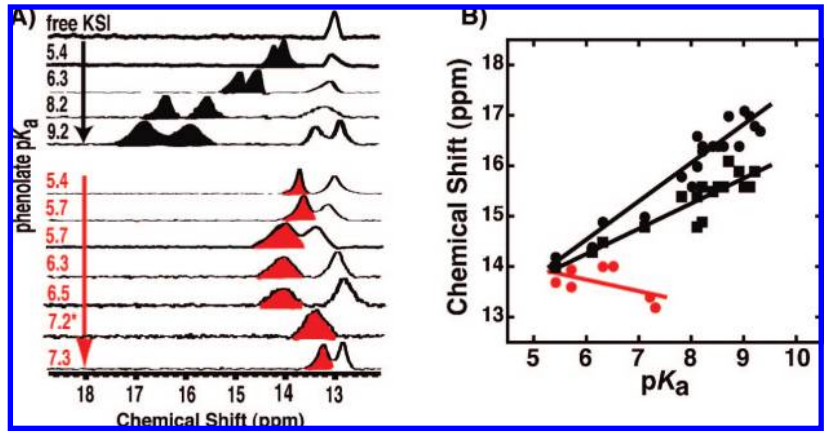

Figure 5. ^{1}H NMR spectra of tKSI^{D40N}·phenolate complexes. (A) Downfield regions of spectra of non-*ortho*-substituted phenolates (black, from ref 45) and DFPs (red) bound to KSI at pH 7.2. Note that the spectrum for 2,4,6-F_3-phenol (pK_a 7.2) was acquired at pH 5.8 due to substantial overlap of the hydrogen-bonded peak with the 13 ppm enzymatic peak at pH 7.2 (see Figure S4). (B) Correlation between increasing phenolate pK_a and chemical shift of the observed downfield hydrogen-bonded proton peak(s). Black symbols represent the two black peaks observed in the non-*ortho*-substituted phenolate spectra in (A) (and additional spectra not shown; data from ref 45), and red symbols represent the downfield peak observed in the DFP spectra in (A) (data from Table S3).

have observed that shortened O···O distances correlate with a more downfield chemical shift of the bridging proton.[69−71] This change in proton chemical shift reflects decreased local magnetic shielding as sigma electron density within the O−H bond moves away from the bridging proton as it migrates toward the acceptor oxygen at shortened O···O distances.[72] Decreased hydrogen bond O···O lengths, enhanced proton migration, and increased downfield chemical shift are expected upon better matching of donor and acceptor proton affinities on the basis of extensive studies of small-molecule complexes by crystallography, NMR and IR spectroscopy, and computation.[49,50,73−76]

Protons involved in hydrogen bonds donated by Y16 and D103 to phenolates substituted only in the *meta* and *para* positions have previously been assigned to downfield peaks detected in ^{1}H NMR spectra of tKSI^{D40N}·phenolate complexes via H−H NOESY spectra, oxyanion hole mutations, and comparison to model compound chemical shifts.[45] These hydrogen-bonded proton peaks move progressively more downfield by up to 3 ppm as the phenolate pK_a increases from 5.4 to 9.3 (Figure 5A,B, black). These changes strongly suggest increased proton migration and a steady shortening of oxyanion hole hydrogen bond O···O distances by ∼0.1 Å in response to increasing charge localization on the phenolate oxygen over the pK_a range of 5.4−9.3. Given the apparent constraints on the positioning of the Y16 and D103 backbone and side chains, shortening of hydrogen bond O···O distances by 0.1 Å is expected to predominantly reflect the combined effects of phenolate C−O bond lengthening with increased oxyanion charge localization and progressive translation of the phenolate deeper into the oxyanion hole. This observation suggests sufficient spatial freedom in the absence of *ortho* substitution to permit phenolate relaxation along the coordinate required for hydrogen bond shortening. These physical changes in enzymatic hydrogen bonds upon better matching of donor and acceptor proton affinities conform to the canonical behavior of O−H···O hydrogen bonds described above.

To test whether di-*ortho*-F-phenolates display altered hydrogen bond behavior, we acquired ^{1}H NMR spectra for a series of DFPs ranging in pK_a from 5.4 to 7.3 (Figure 5A, red). Unlike non-*ortho*-substituted phenolates, for which the protons of both oxyanion hole hydrogen bonds appear as far downfield peaks, DFP binding gives rise to only one downfield peak >13 ppm. This observation suggests that only one of the two oxyanion hole hydrogen bonds inferred from the short O···O distances observed in the X-ray structure involves a deshielded proton that has migrated toward the DFP oxygen. The proton bridging the second hydrogen bond may not have significantly migrated toward the DFP oxygen due to suboptimal orbital overlap with lone-pair electrons on the phenolate oxygen owing to the DFP rotation about the C−O bond axis, as described above. In the absence of significant migration, the bridging proton would be expected to have a chemical shift <11 ppm, rendering it undetectable among the very large number of proton resonances observed in the upfield region of the spectrum. It remains possible, although unlikely, that both hydrogen-bonded protons have identical, overlapping resonances for all DFPs tested. Alternatively, the second hydrogen-bonded proton could be significantly deshielded but undetectable due to broadening from rapid exchange with other groups within the active site, although both hydrogen-bonded protons are observed for non-*ortho* phenolates and have similar peak widths. Additional ^{1}H−^{1}H NOESY and low-pH NMR spectra tested and confirmed assignment of the observed downfield peak to an oxyanion hole hydrogen-bonded proton (Figure S4) but could not further specify whether the peak arises from the Y16 or D103 hydrogen bond. However, the continuous electron density observed in the X-ray structure between the Y16 and DFP oxygens (Figure 1A, visible up to 1.7σ), previously described for linear or nearly linear hydrogen bonds with partial covalent character,[77] is

(69) Jeffrey, G. A.; Yeon, Y. *Acta Crystallogr., Sect. B: Struct. Sci.* **1986**, *42*, 410–413.
(70) Berglund, B.; Vaughan, R. W. *J. Chem. Phys.* **1980**, *73*, 2037–2043.
(71) McDermott, A.; Rydenour, C. F. In *Encyclopaedia of Nuclear Magnetic Resonance*; Grant, D. M., Harris, R. K., Eds.; Wiley: Hoboken, 1996; pp 3820−3824.
(72) Rohlfing, C. M.; Allen, L. C.; Ditchfield, R. *J. Chem. Phys.* **1983**, *79*, 4958–4966.
(73) Gilli, P.; Bertolasi, V.; Pretto, L.; Ferretti, V.; Gilli, G. *J. Am. Chem. Soc.* **2004**, *126*, 3845–3855.
(74) Zundel, G. *Adv. Chem. Phys.* **2000**, *111*, 1–217.
(75) Novak, A. *Structures and Bonding (Berlin, Germany)*; Springer-Verlag: New York, 1974; Vol. 18, pp 177−216.
(76) Brycki, B.; Brzezinski, B.; Zundel, G.; Keil, T. *Magn. Reson. Chem.* **1992**, *30*, 507–510.

Scheme 4. Physical Model for Phenolate Binding in the KSI Oxyanion Hole: (A) Hydrogen Bonds Formed to *Meta*- and *Para*-Substituted Phenolates Shorten with Increasing Phenolate Charge Localization (Indicated by Larger Minus Sign) and (B) O···F Contacts Constrain Hydrogen Bonds Formed to DFPs from Shortening with Increasing Phenolate Charge Localization

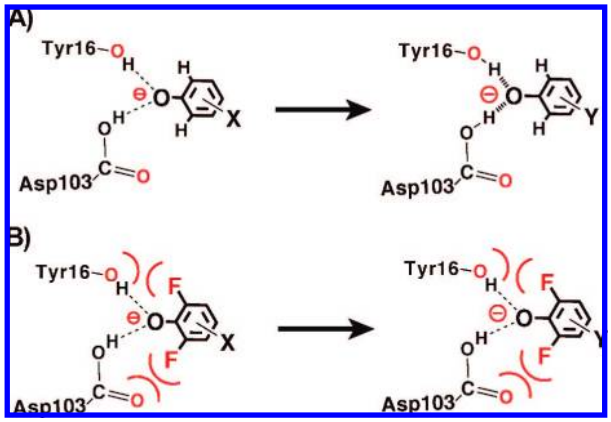

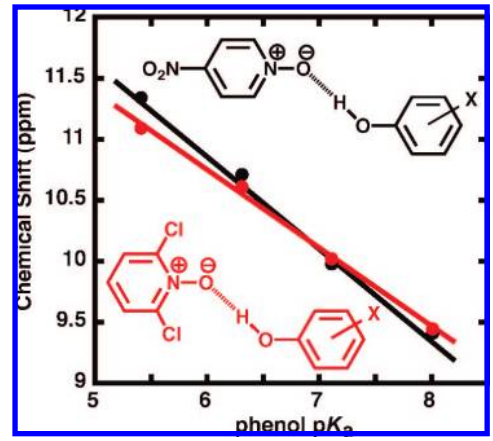

Figure 6. Dependence of the hydrogen-bonded proton chemical shift on phenol pK_a for a series of phenol donors (3,4-dinitrophenol, 3-CF_3-4-nitrophenol, 4-nitrophenol, and 4-cyanophenol) hydrogen-bonded to either 4-nitropyridine-*N*-oxide (black, p$K_a = -1.7$)[81] or 2,6-dichloropyridine-*N*-oxide (red, p$K_a = -2.3$)[82] in chloroform (data from Table S4).

consistent with the observed deshielded proton belonging to this hydrogen bond.

In contrast to the hydrogen bond behavior observed for non-*ortho*-substituted phenolates (Figure 5A,B, black), the chemical shift of the downfield peak observed upon DFP binding did not increase with increasing phenolate pK_a (Figure 5A,B, red). The minimal chemical shift variation from the average value of 13.7 ppm strongly suggests that the bridging proton position and O···O distance within hydrogen bonds formed to DFPs change minimally with increasing phenolate pK_a. Thus, forces arising from the close-packing interactions and putative repulsive O···F contacts identified earlier within the oxyanion hole appear to physically prevent hydrogen bonds formed to DFPs from shortening to the distance they would adopt in the absence of the di-*ortho*-F subsititution (Scheme 4).[78]

To test whether this altered hydrogen bond behavior was indeed imposed by constraints within the enzyme active site and not an inherent property of all hydrogen bonds formed to di-*ortho*-substituted oxyanion acceptors, we characterized the hydrogen bond behavior of small-molecule model complexes in solution. We measured the chemical shift of the hydrogen-bonded proton formed in chloroform between a series of phenol donors and either 4-nitropyridine-*N*-oxide or 2,6-dichloropyridine-*N*-oxide,[79] oxyanionic acceptors of nearly equivalent pK_a. The almost identical chemical shifts observed for hydrogen bonds formed to these acceptors (Figure 6) indicate that di-*ortho*-halo substitution *per se* does not perturb the length of a hydrogen bond or prevent it from shortening. These results are consistent with previous solution studies of intermolecular hydrogen bond formation between trifluoroacetic acid and substituted pyridines[80] in which di-*ortho*- and non-*ortho*-substituted pyridines fell on the same trend line of ^{1}H chemical shift versus pK_a. This identical behavior between di-*ortho*- and non-*ortho*-substituted hydrogen bond acceptors presumably reflects their ability to rotate in solution to avoid unfavorable interactions between the *ortho* substituents and the hydrogen bond donor. Thus, the apparent constraint to shortening hydrogen bonds formed to DFPs bound to KSI is a property of binding interactions within the enzymatic active site.

While it was not possible to test DFPs with pK_a values >7.3 bound to KSI, due to the strong inductive electron withdrawal of the −F substituents themselves, a nearly 2 ppm chemical shift difference is observed at pK_a 7.3 for DFPs relative to non-*ortho*-phenolates of equivalent pK_a (Figure 5B). Extensive studies of O−H···O hydrogen bonds in small-molecule complexes have identified a strong correlation between the hydrogen bond O···O distance and the chemical shift of the bridging proton, with the chemical shift increasing from 12 to 20 ppm as the O···O distance decreases from ~2.70 to 2.45 Å.[69−71,83] A conservative upper limit for an increase in the chemical shift of DFPs of ~0.5 ppm with increasing pK_a would correspond to a hydrogen bond shortening of at most 0.02 Å. This behavior is in contrast to the ~2 ppm chemical shift increase observed for non-*ortho*-phenolates over the same pK_a range and the 0.07 Å change in hydrogen bond length calculated from the correlation function in ref 83. Thus, the forces in and surrounding the oxyanion hole can constrain the O···O distance of hydrogen bonds formed to bound DFPs from shortening over distances on the scale of ~0.1 Å (Scheme 4). *Ab initio* gas-phase calculations on the formate−formic acid dimer suggest that lengthening a single O···O hydrogen bond 0.1 Å from its optimal distance weakens the hydrogen bond by 1.2 kcal/mol.[84] Does constraining KSI oxyanion hole hydrogen bonds formed to DFPs from shortening by up to 0.1 Å substantially weaken phenolate binding? We turned to direct measurement of the change in binding affinity across a series of fluorophenolates

(77) Stevens, E. D.; Lehmann, M. S.; Coppens, P. *J. Am. Chem. Soc.* **1977**, *99*, 2829–2831.
(78) The nearly identical downfield chemical shifts observed for di-*ortho*-fluorophenolates of similar pK_a but with very different *meta* or *para* substituents (see Table S3) suggest that the remote substituents themselves do not contribute substantially to the observed constraint on hydrogen bond shortening.
(79) Pyridine-*N*-oxides were used as oxyanionic hydrogen bond acceptors instead of phenolates since they did not require the presence of a counterion. The dichloro compound was used instead of the difluoro variant due to the commercial availability of the former.
(80) Dega-Szafran, Z.; Dulewicz, E. *J. Chem. Soc., Perkin Trans. 2* **1983**, 345–352.
(81) Jencks, W. P.; Regenstein, J. In *Handbooks of Biochemistry and Molecular Biology*; Fasman, G. D., Ed.; CRC Press: Cleveland, 1976; pp 305−351.
(82) Johnson, C. D.; Katritzky, A. R.; Shakir, N. *J. Chem. Soc. B* **1967**, 1235–1237.
(83) Harris, T. K.; Mildvan, A. S. *Proteins* **1999**, *35*, 275–282.
(84) Kumar, G. A.; Pan, Y.; Smallwood, C. J.; McAllister, M. A. *J. Comput. Chem.* **1998**, *19*, 1345–1352.

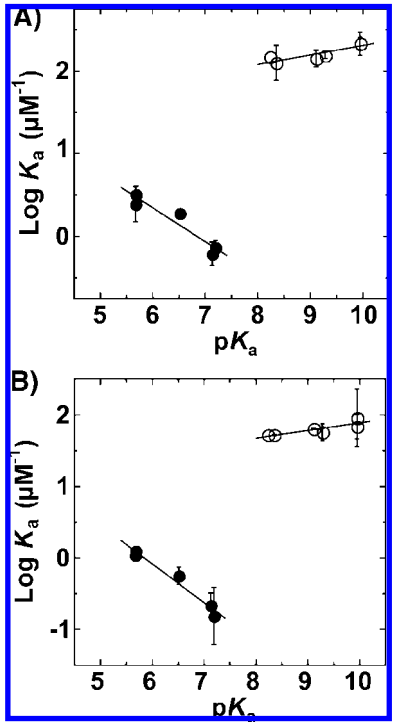

Figure 7. Energetics of fluorophenolate binding to KSI^{D40N}: the dependence of affinity (log K_a) on the pK_a of non-*ortho*-fluorophenolates (open circles; from ref 45) and di-*ortho*-fluorophenolates (filled circles) for binding to pKSI (A) and tKSI (B). Slopes for pKSI are 0.11 ± 0.03 and −0.41 ± 0.08, and those for tKSI are 0.10 ± 0.03 and −0.54 ± 0.06. (Data from Table S5.)

of increasing phenolate pK_a to directly and quantitatively assess the energetic consequence of di-*ortho*-F substitution and active-site constraints to hydrogen bond shortening.

Constrained Hydrogen Bonding Substantially Weakens Ligand Binding and Negative Charge Stabilization within the KSI Oxyanion Hole. As discussed earlier, the oxyanion hole binding of a series of *meta*- and *para*-substituted fluorophenolates of increasing pK_a and negative charge character resulted in a small increase in binding affinity ($\Delta\Delta G$) by 0.2 kcal/mol per unit increase in phenolate pK_a (Figure 7, open circles).[45] If hydrogen bond shortening up to 0.1 Å with increasing phenolate pK_a makes a substantially favorable energetic contribution to phenolate binding and negative charge stabilization (which may be nearly offset by concomitant unfavorable dipolar rearrangements within the active site, as discussed earlier),[45] then the observed geometric constraints arising from di-*ortho*-F substitution that prevent hydrogen bond shortening would be predicted to result in weakened phenolate binding at increased pK_a. Conversely, if hydrogen bond shortening by this magnitude makes a negligible energetic contribution, then the trend in $\Delta\Delta G$ would be similar to that previously observed with *meta*- and *para*-substituted fluorophenolates.

Figure 7 shows the dependence of the association constant (log K_a), determined by a fluorescence competitive binding assay, on the pK_a of non-*ortho*- (open circles) or di-*ortho*-fluorophenolates (filled circles) obtained for KSI from two different bacterial sources (Figure 7A,B). At a pK_a of 7, interactions arising from introduction of the di-*ortho*-F atoms weakens phenolate binding by 3 kcal/mol relative to that expected from extrapolation for a non-*ortho*-fluorophenolate of identical pK_a. This absolute difference in observed binding reflects the combined and convoluted energetic effects of constrained hydrogen bond shortening, O···F repulsions, rotation of the DFP ring, and any differential solvation of the *ortho*-F atoms within the active site relative to water. Furthermore, this affinity difference for binding to the KSI active site is in sharp contrast to solution studies of intermolecular hydrogen bond formation between 4-Br-phenol and substituted phenolates, in which di-*ortho*-substituted phenolates fell on the same trend line of log K_a versus pK_a as non-*ortho*-substituted phenolates.[85] This identical behavior presumably reflects the ability of di-*ortho*-phenolates to rotate in solution to avoid unfavorable interactions between the *ortho* substituents and hydrogen bond donor groups, as suggested by the quantum calculations presented earlier of the energy-minimized gas-phase structure for hydrogen bond formation to DFP (Figure 2B) and the proton chemical shift behavior of the hydrogen-bonded complexes in solution (Figure 6).

Although the absolute binding affinity (ΔG) of a DFP at any given pK_a reflects many complex physical changes within the active site, the *change* in binding affinity per *change* in DFP pK_a ($\Delta\Delta G$) is expected to primarily report on those changes within the active site that occur in response to increasing or decreasing negative charge localization on the DFP oxygen. While the dependence of the affinity on pK_a ($\Delta\Delta G$) is shallow and slightly positive for the non-*ortho*-fluorophenolates (∼0.1, $\Delta\Delta G$ = 0.2 kcal/mol/pK_a unit), the slope is steeply negative for the di-*ortho*-fluorophenolates (−0.4 to −0.5; $\Delta\Delta G$ = −0.6 to −0.7 kcal/mol/pK_a unit). This result indicates that, over the pK_a ranges studied, increased charge localization on the DFP oxyanion equivalent to a 1 pK_a unit increase weakens binding by ∼1 kcal/mol relative to phenolates lacking di-*ortho*-F atoms. Thus, geometric constraints within the KSI active site that occur as a consequence of di-*ortho*-F substitution and constrain hydrogen bonds formed to the DFP oxygen from shortening up to 0.1 Å substantially impair the ability of the active site to stabilize increased oxyanion charge localization relative to water. This result confirms the prediction made by the KSI active-site model presented earlier, in which the systematic shortening of hydrogen bonds formed to the incipient oxyanion of bound phenolates of increasing pK_a makes an energetically substantial contribution to negative charge stabilization within the active site.[45] Indeed, electrostatic interactions between the phenolate oxygen and preorganized dipoles present within the remainder of the active site are insufficient to offset the observed weakening in phenolate binding when oxyanion hole hydrogen bonds are constrained from shortening.

Conclusions and Implications

Polanyi, Pauling, Haldane, Jencks, and others recognized that a fundamental difference between carrying out reactions within enzyme active sites and in aqueous solution is the ability of enzymes to exploit noncovalent binding interactions to position substrates with respect to one another and relative to reactive functional groups.[6−9] Indeed, the myriad three-dimensional structures of enzyme·substrate complexes solved to date have highlighted the general complementarity between active sites and reactants.[86] It has been broadly proposed that enzymes use positioning to achieve selective transition-state stabilization by forming stronger binding interactions with the transition state than the ground state, based on geometric changes in the reacting

(85) Kolthoff, I. M.; Chantooni, M. K., Jr. *J. Am. Chem. Soc.* **1969**, *91*, 4621–4625.
(86) Kahraman, A.; Morris, R. J.; Laskowski, R. A.; Thornton, J. M. *J. Mol. Biol.* **2007**, *368*, 283–301.

substrate that allow more stabilizing contacts to form in one state than another.[9,13,87−90] However, the distance scale on which enzymes can distinguish geometric rearrangement and the energetic significance of any discrimination on that scale remained unanswered questions that are fundamental to our most basic physical understanding of enzyme active sites and catalysis.

Multiple prior studies have used Glu-to-Asp mutations to test the importance of positioning reactive carboxylate groups relative to substrates. Such mutations, which remove a methylene group and perturb the positioning of the carboxylate by ∼1 Å,[91,92] are associated with reductions in enzyme activity as large as 10^4-fold.[93−96] It was unclear, however, whether geometric changes less than 1 Å in magnitude, such as those occurring within reacting substrates along the reaction coordinate (Scheme 1),[20] could be recognized by enzymes and whether such discriminations would be energetically important. Evidence that substantial geometric discrimination on this scale might be possible was provided by the surprisingly large reductions in catalysis observed upon oxygen-to-sulfur substitutions of key groups in several enzymes, highlighting the potential of the 0.3 Å longer covalent bond and larger van der Waals radius of S relative to O to disrupt the alignment and positioning of active-site contacts important for catalysis.[10,97−100] Nevertheless, the observed rate effects from O/S substitutions are not solely a reflection of subtle geometric perturbations but can be convoluted with additional effects due to the altered chemical properties of S relative to O.

We have reported herein a selective test of the limits of structural precision and geometrical discrimination possible within the active site of a particular enzyme, bacterial ketosteroid isomerase. The results provide strong evidence that forces arising from noncovalent packing and binding interactions within this active site can constrain the positioning of a bound phenolate ligand and contacting side chains with a precision of ±0.1 Å or better. These constraints are sufficient to prevent relaxation of side-chain and ligand positions along the specific coordinate required for shortening of oxyanion hole hydrogen bond O···O distances by ∼0.1 Å upon increased charge localization. The structural rigidity within the KSI active site that enables geometric discrimination on this scale appears to derive from tight packing of hydrophobic groups around D103 and Y16 that limits the rotational rearrangement and thermal mobility of these groups, coupled with structural constraints in the substrate binding pocket. While the amplitude of zero-point bond vibrations, which represent the minimum temperature-independent mobility of covalently bonded atoms, are on the same scale as the ∼0.1 Å geometric constraints observed in KSI, vibrational modes are highly anisotropic, and rotational modes can be highly constrained.[41,42] More limited atomic motions on scales less than 0.1 Å within the oxyanion hole along specific trajectories orthogonal to allowed motional modes may enhance rigidity along the coordinate needed to constrain hydrogen bond shortening by up to 0.1 Å. Local flexibility may be further dampened by simultaneous motions of neighboring atoms toward each other that result in unfavorable van der Waals overlap, thereby limiting the amplitude of motions in a particular direction. Such motions are sometimes referred to as "anticorrelated",[101] and similar effects for the KSI active site have been reported based on MD simulations.[102]

Geometric constraints in KSI that prevent side-chain and ligand structural relaxation by ∼0.1 Å have substantial energetic consequences. Indeed, increased charge localization on the phenolate oxygen equivalent to a 1 pK_a unit increase weakens binding by ∼1 kcal/mol relative to phenolates lacking di-*ortho*-F atoms. This energetic difference over the limited pK_a range tested suggests that, over a much larger pK_a range of 10−15 units, such as that traversed in going from the ground state to transition state during steroid isomerization, the presence or absence of geometric constraints akin to those resulting in this system from di-*ortho*-F substitution could lead to differential stabilization energies and binding affinities of several kilocalories per mole.

While the specific physical interactions underlying the geometric constraints described in this study are distinct from interactions during catalysis by KSI, they are conceptually related to the types of geometric discriminations that have been proposed to make significant contributions to selective transition-state stabilization in KSI,[45] serine proteases and other oxyanion hole-containing hydrolases,[14−16,103,104] and phosphoryl-transfer enzymes.[19,22,23,105] In all of these cases, the rigid positioning of active-site residues has been proposed to constrain favorable interactions from forming in the ground state but permit them to form in the transition state once geometric constraints have been relieved due to changes in the hybridization of substrate atoms.

In the case of KSI, structural features of the oxyanion hole suggest that hydrogen bond formation to the reacting substrate is geometrically optimal in the transition state but not in the ground state. During steroid isomerization, the hybridization of the substrate oxygen changes from a planar sp^2 carbonyl to a tetrahedral sp^3 dienolate (Scheme 3A), altering the spatial distribution of its lone pair electrons. This reorientation of atomic orbitals about the substrate oxygen alters its geometric preference for accepting hydrogen bonds. Whereas the ground-state carbonyl preferentially accepts hydrogen bonds within the sp^2

(87) Wells, T. N. C.; Fersht, A. R. *Biochemistry* **1986**, *25*, 1881–1886.
(88) Leatherbarrow, R. J.; Fersht, A. R.; Winter, G. *Proc. Natl. Acad. Sci. U.S.A.* **1985**, *82*, 7840–7844.
(89) Miller, B. G.; Wolfenden, R. *Annu. Rev. Biochem.* **2002**, *71*, 847–885.
(90) Robertus, J. D.; Alden, R. A.; Birktoft, J. J.; Kraut, J.; Powers, J. C.; Wilcox, P. E. *Biochemistry* **1972**, *11*, 2439–2449.
(91) Joseph-McCarthy, D.; Rost, L. E.; Komives, E. A.; Petsko, G. A. *Biochemistry* **1994**, *33*, 2824–2829.
(92) Debler, E. W.; Ito, S.; Seebeck, F. P.; Heine, A.; Hilvert, D.; Wilson, I. A. *Proc. Natl. Acad. Sci. U.S.A.* **2005**, *102*, 4984–4989.
(93) Raines, R. T.; Sutton, E. L.; Straus, D. R.; Gilbert, W.; Knowles, J. R. *Biochemistry* **1986**, *25*, 7142–7154.
(94) Alter, G. M.; Casazza, J. P.; Wang, Z.; Nemeth, P.; Srere, P. A.; Evans, C. T. *Biochemistry* **1990**, *29*, 7557–7563.
(95) Lawson, S. L.; Wakarchuk, W. W.; Withers, S. G. *Biochemistry* **1996**, *35*, 10110–10118.
(96) Seebeck, F. P.; Hilvert, D. *J. Am. Chem. Soc.* **2005**, *127*, 1307–1312.
(97) Polgar, L.; Bender, M. L. *Biochemistry* **1967**, *6*, 610–620.
(98) Neet, K. E.; Nanci, A.; Koshland, D. E., Jr. *J. Biol. Chem.* **1968**, *243*, 6392–6401.
(99) Zhang, Y. L.; Hollfelder, F.; Gordon, S. J.; Chen, L.; Keng, Y. F.; Wu, L.; Herschlag, D.; Zhang, Z. Y. *Biochemistry* **1999**, *38*, 12111–12123.
(100) Brautigam, C. A.; Steitz, T. A. *J. Mol. Biol.* **1998**, *277*, 363–377.
(101) Luo, J.; Bruice, T. C. *Proc. Natl. Acad. Sci. U.S.A.* **2004**, *101*, 13152–13156.
(102) Mazumder, D.; Kahn, K.; Bruice, T. C. *J. Am. Chem. Soc.* **2003**, *125*, 7553.
(103) Valina, A. L.; Mazumder-Shivakumar, D.; Bruice, T. C. *Biochemistry* **2004**, *43*, 15657–15672.
(104) Wilmouth, R. C.; Westwood, N. J.; Anderson, K.; Brownlee, W.; Claridge, T. D.; Clifton, I. J.; Pritchard, G. J.; Aplin, R. T.; Schofield, C. J. *Biochemistry* **1998**, *37*, 17506–17513.
(105) Rupert, P. B.; Massey, A. P.; Sigurdsson, S. T.; Ferre-D'Amare, A. R. *Science* **2002**, *298*, 1421–1424.

orbital plane of the carbonyl group, optimal orbital overlap and hydrogen bond formation to the dienolate intermediate occur above and below the plane of the steroid and C−O bond. However, the D103 and Y16 side chains appear consistently positioned above and below the plane of the steroid and C−O bond in previously published structures with bound transition-state analogues[45,106] (Figure 1C) and are identically oriented in structures of unliganded KSI.[107] This invariance of D103 and Y16 orientations is consistent with tight packing of the surrounding hydrophobic residues and constraints on side-chain positioning. Furthermore, a preliminary X-ray structure of KSI containing a bound product analogue indicates that the carbonyl group is positioned within the oxyanion hole such that the carbonyl oxygen accepts hydrogen bonds that are substantially out of the sp^2 orbital plane (unpublished results). Empirically derived and quantum mechanical potential energy functions for hydrogen bond formation to oxygen acceptors suggest that significant energetic discrimination may be possible from positioning hydrogen bond donors within the KSI oxyanion hole for optimal interaction with the transition state rather than the ground state.[108,109] Indeed, energetic measurements indicate that oxyanion hole mutations that reduce catalysis have proportional effects on transition-state analogue binding affinity but have no effect on product analogue binding (unpublished results).

Favorable features of KSI permitted a selective test of the scale of geometrical discrimination and accompanying energetic consequences possible in this particular enzyme active site. Multifaceted structural, spectroscopic, computational, and energetic tests of enzyme function, similar to the approaches taken herein, will be necessary to test the generality of our conclusions, to broaden our understanding of geometric effects in other enzymatic systems, and ultimately to garner a full understanding of the catalytic power of enzymes.

Methods

Materials. All reagents were of the highest purity commercially available (≥97%). Substituted phenols and pyridine-*N*-oxides were purchased from Sigma-Aldrich, Oakwood Products, and Acros Organics. All buffers were prepared with reagent-grade chemicals or better.

KSI Expression and Purification. KSI was expressed and purified as previously described.[45] Final purity was >99%, as estimated from a Coomassie-stained SDS−PAGE gel, and protein concentration was determined using the calculated molar extinction coefficient in 6 M guanidium chloride.[110]

Absorbance Spectra of KSI·2,6-Difluorophenolate Complexes. Absorbance spectra of substituted 2,6-F_2-phenolates were acquired in a microcuvette with a Uvikon 9310 absorbance spectrophotometer. Spectra of 50 μM phenols in 10 mM HCl (pH 2) and 10 mM NaOH (pH 12) were compared with the spectrum of the same concentration phenol in 40 mM potassium phosphate (KP_i) buffer, pH 7.2, in the presence of 300 μM $tKSI^{D40N}$ (phenol >95% bound, data not shown) after subtraction of the free enzyme spectrum.

KSI X-ray Crystallography. $pKSI^{D40N}$·2,6-difluorophenolate and $pKSI^{D40N}$·2-fluorophenolate cocrystals in space group $C222_1$ were obtained using the hanging drop vapor diffusion method by mixing 2 μL of $pKSI^{D40N}$ at 25 mg/mL and 2 μL of reservoir solution (1.4 M ammonium sulfate, 6.5% (v/v) 2-propanol, and 2−3 mM 2,6-difluorophenol or 2-fluorophenol at pH 7.0). Cube-shaped crystals measuring ~0.4 mm × 0.4 mm × 0.3 mm appeared after one week of incubation at room temperature. Cryo-protection was achieved by first soaking the crystals in a solution of mother liquor diluted 1:1 with 2.9 M sodium malonate (pH 7.0) and then transferring the crystals directly into the 2.9 M sodium malonate solution. Crystals were shock-cooled by immersion into liquid nitrogen. Diffraction data from single crystals maintained at 100 K were collected for $pKSI^{D40N}$·2,6-difluorophenolate at beamline 14-BMC of the Advanced Photon Source (Argonne National Laboratory, Argonne, IL) and for $pKSI^{D40N}$·2-fluorophenolate at beamline BL9-1 of the Stanford Synchrotron Radiation Laboratory (Stanford Linear Accelerator Center, Stanford, CA). Data were integrated and scaled using the HKL2000 program package.[111] An initial model of the protein was obtained by the molecular replacement method with the program PHASER,[112] using the coordinates of a previously reported structure of $pKSI^{D40N}$ (PDB code 2PZV). Refinement and manual rebuilding were carried out using the programs REFMAC5[113] and COOT,[114] respectively. Model quality was assessed using the program PROCHECK,[115] and the Ramachandran plot showed no residues outside the allowed regions. For the $pKSI^{D40N}$·2-fluorophenolate structure, the occupancy of 2-fluorophenolate was reduced from 100% to 60%, with a water molecule occupying the oxyanion hole with an occupancy of 40%, to properly account for the observed electron density of the ligand in the active site. Data and model statistics are included as Table S1 ($pKSI^{D40N}$·2,6-difluorophenolate) and Table S2 ($pKSI^{D40N}$·2-fluorophenolate) in the Supporting Information. Structural coordinates have been deposited in the RCSB Protein Data Bank (http://www.rcsb.org/pdb) under accession codes 2INX ($pKSI^{D40N}$·2,6-difluorophenolate) and 3CPO ($pKSI^{D40N}$·2-fluorophenolate).

KSI NMR Spectroscopy. ^{1}H NMR spectra of KSI were acquired at the Stanford Magnetic Resonance Laboratory on an 800-MHz Varian ^{UNITY}INOVA spectrometer running VNMR v6.1C and equipped with a 5-mm, triple-resonance, gradient $^1H(^{13}C/^{15}N)$ probe. NMR samples consisted of 0.5−2.0 mM $tKSI^{D40N}$ and 0.5−5.0 mM substituted phenol in 40 mM KP_i buffer (pH 7.2), 1 mM EDTA, 2 mM DTT, and 10% (v/v) DMSO-d_6 (which served as the deuterium lock solvent and prevented freezing at subzero temperatures) in 5 mM Shigemi symmetrical microtubes at −3.0 ± 0.5 °C. One-dimensional proton spectra were acquired using the 1331 binomial pulse sequence[116] to suppress the water signal, with a spectral width of 30 ppm (carrier frequency set on the water resonance) and an excitation maximum of 14−17 ppm. Data were collected with 32 000 points and a 1.9 s recycle delay for 512−5120 scans and processed using a 10-Hz line broadening, with a baseline correction applied over the peaks of interest. Chemical shifts were referenced internally to the water resonance (5.1 ppm at −3 °C) and externally to a sample of sodium 3-trimethylsilylpropionate-2,2,3,3-d_4 (0 ppm) in the same buffer conditions and were reproducible to ±0.1 ppm in independent samples.[117] As previously described, spectra were consistent with slow exchange on the NMR time scale.[45]

Two dimensional ^{1}H−^{1}H NOESY spectra were acquired using the SS-NOESY pulse sequence to minimize saturation of protons

(106) Cho, H. S.; Ha, N. C.; Choi, G.; Kim, H. J.; Lee, D.; Oh, K. S.; Kim, K. S.; Lee, W.; Choi, K. Y.; Oh, B. H. *J. Biol. Chem.* **1999**, *274*, 32863–32868.
(107) Cho, H. S.; Choi, G.; Choi, K. Y.; Oh, B. H. *Biochemistry* **1998**, *37*, 8325–8330.
(108) Lommerse, J. P. M.; Price, S. L.; Taylor, R. *J. Comput. Chem.* **1997**, *18*, 757–774.
(109) Kortemme, T.; Morozov, A. V.; Baker, D. *J. Mol. Biol.* **2003**, *326*, 1239–1259.
(110) Gill, S. C.; von Hippel, P. H. *Anal. Biochem.* **1989**, *182*, 319.
(111) Otwinowski, Z.; Minor, W. *Macromol. Crystallogr. A* **1997**, *276*, 307–326.
(112) Mccoy, A. J.; Grosse-Kunstleve, R. W.; Adams, P. D.; Winn, M. D.; Storoni, L. C.; Read, R. J. *J. Appl. Crystallogr.* **2007**, *40*, 658–674.
(113) Murshudov, G. N.; Vagin, A. A.; Dodson, E. J. *Acta Crystallogr., Sect. D: Biol.Crystallogr.* **1997**, *53*, 240–255.
(114) Emsley, P.; Cowtan, K. *Acta Crystallogr., Sect. D: Biol. Crystallogr.* **2004**, *60*, 2126–2132.
(115) Laskowski, R. A.; MacArthur, M. W.; Moss, D. S.; Thornton, J. M. J. *Appl. Crystallogr.* **1993**, *26*, 283–291.
(116) Turner, D. L. *J. Magn. Reson.* **1983**, *54*, 146–148.

exchanging with bulk water.[118] Data were acquired over 23.8 ppm spectral widths of 2048 data points with a 50 ms mixing time, 1.55 s recycle delay, and 64 scans per t_1 increment over 256 increments. Spectra were processed using shifted, squared sine bell window functions in both dimensions and one-fold zero-filling in the t_1 dimension and viewed with the program SPARKY.[119]

One-dimensional ^{19}F spectra of tKSI^{D40N}-bound F-phenolates were acquired on a 500-MHz Varian ^{UNITY}INOVA NMR spectrometer (operating at 470.23-MHz) running VNMR v6.1C and equipped with a 5-mm PFG switchable probe operating at ambient temperature (20 °C). Here, 10% (v/v) D_2O served as the lock solvent, and ^{19}F chemical shifts were referenced to an external standard of trifluoroacetic acid (−76.1 ppm relative to $CFCl_3$). Spectra for 20 mM free phenols were obtained (12 scans) in 10 mM NaOH (pH 12), a condition in which each phenol is present as the ionized phenolate. A total of 200−4000 scans were obtained for each tKSI^{D40N}-bound phenol under conditions in which the phenol was >95% bound (40 mM KP_i, 1 mM EDTA, 2 mM DTT, 1.5 mM enzyme, 1 mM phenol, data not shown) and processed using a 10 Hz line broadening with a baseline correction applied over the observed peaks.

^{1}H NMR of Small-Molecule Hydrogen-Bonded Complexes. ^{1}H NMR spectra were acquired at −45 °C on a 400 MHz Varian Mercury NMR spectrometer equipped with a 5-mm PFG autoswitchable four-nucleus (^{13}C/^{31}P−^{1}H/^{19}F) probe and running VNMR v6.1C. Samples of 1:1 hydrogen-bonded complexes (50 mM) were prepared in $CDCl_3$ (with 0.05% TMS for referencing) and contained either 4-NO_2-pyridine-*N*-oxide or 2,6-Cl_2-pyridine-*N*-oxide as the hydrogen bond acceptor and 3,4-$(NO_2)_2$-phenol, 3-CF_3-4-NO_2-phenol, 4-NO_2-phenol, or 4-CN-phenol as the hydrogen bond donor. Spectra were taken (25−100 scans) for each hydrogen-bonded complex, and the data were processed using a line broadening of 5 Hz.

Determination of Phenolate Affinities for KSI. Fluorophenolate affinities for KSI were determined using a fluorescence competition binding assay described previously.[45] Briefly, the KSI affinity of EqA488-1, the KSI reaction intermediate analogue equilenin conjugated to Alexa Fluor 488, was determined by titration with enzyme using a a FluoroLog-3 spectroflourometer to monitor quenching of the Alexa Fluor fluorescence upon binding to KSI (excitation at 480 nm, emission at 515 nm, bandpass of 10 and 14.7 nm, respectively, and 0.1 nM EqA488-1 in a 45 μL microcuvette). Enzyme concentration (typically 0.1−100 nM) was varied above and below the K_d for the ligand (~1 nM for EqA488-1). After correction for background fluorescence, the observed EqA488-1 fluorescence as a function of enzyme concentration was fit to a quadratic binding isotherm using nonlinear regression analysis to determine the EqA488-1 affinity for KSI, as previously described.[45] The EqA488-1 K_d of 1.0 nM determined by this method was the same as previously reported.[45]

To determine the observed KSI affinities for the series of 2,6-F_2-phenol ligands (with varying fluorine substitution at the other ring positions) by competition, EqA488-1 was displaced from the active site of KSI by the addition of the substituted 2,6-F_2-phenol to a mixture of the enzyme (with concentration 1−4-fold above the EqA488-1 K_d) and EqA488-1 (0.1 nM). The observed fluorescence as a function of phenol concentration was fit to a quadratic binding isotherm, and the KSI affinity of the 2,6-F_2-phenol ligand under assay conditions along with the pH-independent KSI affinity of the substituted 2,6-F_2-phenolate were determined as previously described.[45] Error bars are the average deviation of 2−6 independent assays.

Quantum Mechanical Calculations. Energy minimization and geometry optimization of the isolated 2,6-F_2-phenolate ligand receiving hydrogen bonds from the Y16 and protonated D103 side chains were performed with the B3LYP density functional method and the 6-311++G(d,p) basis set using the Gaussian 03 software package.[120] Initial side-chain and ligand coordinates were obtained from the pKSI^{D40N}·phenolate X-ray structure (PDB code 2PVZ). The side chains were each truncated at their respective C_β atoms by converting the methylene group into a methyl group, thereby modeling Y16 as 4-Me-phenol and D103 as acetic acid, and −F atoms were added to both *ortho* positions of the phenolate ligand. Side-chain positions were fixed with respect to each other, while the DFP position and orientation were permitted to vary during all calculations.

Acknowledgment. We thank Corey Liu and Steve Lynch for assistance with NMR experiments; Tzanko Doukov for help with crystallographic data collection at SSRL; Dave Agard, Steve Boxer, Aaron Fafarman, Pehr Harbury, Chaitan Khosla, Judith Klinman, Jonathan Lassila, and Jason Schwans for helpful discussions; and members of the Herschlag laboratory for comments on the manuscript. This work was funded by an NSF grant to D.H., D.R., and G.A.P. (MCB-0641393). P.A.S. and D.A.K. were supported in part by HHMI Predoctoral Fellowships. Use of the Advanced Photon Source was supported by the U.S. Department of Energy, Office of Science, Office of Basic Energy Sciences, under Contract DE-AC02-06CH11357. Use of the Stanford Magnetic Resonance Laboratory was supported in part by the Stanford University School of Medicine. Use of the Stanford Synchrotron Radiation Laboratory was supported by the Department of Energy, Office of Biological and Environmental Research, and by the National Institutes of Health, National Center for Research Resources, Biomedical Technology Program, and the National Institute of General Medical Sciences.

Supporting Information Available: Complete ref 119; UV absorbance spectra for tKSI^{D40N}·DFP complexes (Figure S1); atomic B-factors for the pKSI^{D40N}·phenolate (Figure S2A) and pKSI^{D40N}·2-F-phenolate (Figure S2B) structures; electron density map of pKSI^{D40N}·2-F-phenolate oxyanion hole (Figure S3); ^{1}H−^{1}H NOESY and low-pH NMR spectra for tKSI^{D40N}·phenolate complexes (Figure S4); data collection and crystallographic refinement statistics for the pKSI^{D40N}·2,6-F_2-phenolate (Table S1) and pKSI^{D40N}·2-F-phenolate X-ray structures (Table S2); ^{1}H NMR chemical shifts of downfield peaks in spectra of tKSI^{D40N}·DFP complexes (Table S3); ^{1}H NMR chemical shifts of hydrogen-bonded proton observed for complexes between substituted phenols and 4-nitropyridine-*N*-oxide or 2,6-dichloropyridine-*N*-oxide (Table S4); and binding affinities of DFPs to KSI^{D40N} determined by fluorescence (Table S5). This material is available free of charge via the Internet at http://pubs.acs.org.

JA803928M

(117) Wishart, D. S.; Bigam, C. G.; Yao, J.; Abildgaard, F.; Dyson, H. J.; Oldfield, E.; Markley, J. L.; Sykes, B. D. *J. Biomol. NMR* **1995**, *6*, 135–140.
(118) Smallcombe, S. H. *J. Am. Chem. Soc.* **1993**, *115*, 4776–4785.
(119) Goddard, T. D.; Kneller, D. G. *SPARKY*; University of California: San Francisco, 2004.
(120) Frisch, M. J.; et al. *Gaussian 03*, Revision C.02; Gaussian, Inc.: Wallingford, CT, 2004.